University of Groningen

The Dynamics of Complex Formation between Amy lose Brushes on Gold and Fatty Acids by QCM-D

Cao, Zheng; Tsoufis, Theodoros; Svaldo-Lanero, Tiziana; Duwez, Anne-Sophie; Rudolf, Petra; Loos, Katja

Published in:
Biomacromolecules

DOI:
10.1021/bm4010904

IMPORTANT NOTE: You are advised to consult the publisher's version (publisher's PDF) if you wish to cite from it. Please check the document version below.

Document Version
Publisher's PDF, also known as Version of record

Publication date:
2013

Link to publication in University of Groningen/UMCG research database

Citation for published version (APA):
Cao, Z., Tsoufis, T., Svaldo-Lanero, T., Duwez, A-S., Rudolf, P., & Loos, K. (2013). The Dynamics of Complex Formation between Amy lose Brushes on Gold and Fatty Acids by QCM-D. *Biomacromolecules*, *14*(10), 3713-3722. https://doi.org/10.1021/bm4010904

Copyright
Other than for strictly personal use, it is not permitted to download or to forward/distribute the text or part of it without the consent of the author(s) and/or copyright holder(s), unless the work is under an open content license (like Creative Commons).

The publication may also be distributed here under the terms of Article 25fa of the Dutch Copyright Act, indicated by the "Taverne" license. More information can be found on the University of Groningen website: https://www.rug.nl/library/open-access/self-archiving-pure/taverne-amendment.

Take-down policy
If you believe that this document breaches copyright please contact us providing details, and we will remove access to the work immediately and investigate your claim.

Downloaded from the University of Groningen/UMCG research database (Pure): http://www.rug.nl/research/portal. For technical reasons the number of authors shown on this cover page is limited to 10 maximum.

Article

pubs.acs.org/Biomac

The Dynamics of Complex Formation between Amylose Brushes on Gold and Fatty Acids by QCM-D

Zheng Cao,[†] Theodoros Tsoufis,[†] Tiziana Svaldo-Lanero,[‡] Anne-Sophie Duwez,[‡] Petra Rudolf,*[,†] and Katja Loos*[,†]

[†]Zernike Institute for Advanced Materials, University of Groningen, Nijenborgh 4, NL-9747 AG Groningen, The Netherlands

[‡]Department of Chemistry, University of Liège, B6a Sart-Tilman, 4000 Liège, Belgium

Supporting Information

ABSTRACT: Amylose brushes were synthesized by enzymatic polymerization with glucose-1-phosphate as monomer and rabbit muscle phosphorylase b as catalyst on gold-covered surfaces of a quartz crystal microbalance. Fourier transform infrared (FT-IR) spectra confirmed the presence of the characteristic absorption peaks of amylose between 3100 cm^{-1} and 3500 cm^{-1}. The thickness of the amylose brushes—measured by Spectroscopic Ellipsometry—can be tailored from 4 to 20 nm, depending on the reaction time. The contour length of the stretched amylose chains on gold surfaces has been evaluated by single molecule force spectroscopy, and a total chain length of about 20 nm for 16.2 nm thick amylose brushes was estimated. X-ray photoelectron spectroscopy (XPS) was employed to characterize the amylose brushes before and after the adsorption of fatty acids. The dynamics of inclusion complex formation between amylose brushes and two fatty acids (octanoic acid and myristic acid) with different chain length was investigated as a function of time using a quartz crystal microbalance with dissipation monitoring (QCM-D) immersed in the liquid phase. QCM-D signals including the frequency and dissipation shifts elucidated the effects of the fatty acid concentration, the solvent types, the chain length of the fatty acids and the thickness of the amylose brushes on the dynamics of fatty acid molecule adsorption on the amylose brush-modified sensor surfaces.

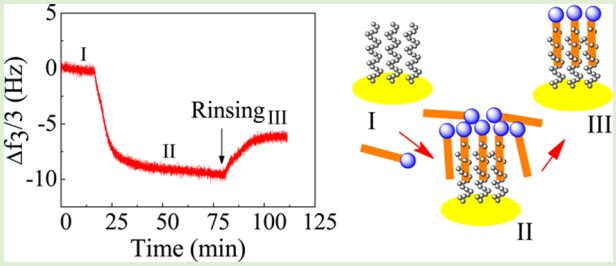

INTRODUCTION

Amylose, one component of starch, is a linear polymer in which the glucose units are linked via α-(1→4) glucosidic linkages. It can adopt a single helical structure to form inclusion complexes with various guest molecules such as iodine,[1,2] lipids,[3] alcohols,[4] and polymers[5,6] via hydrophobic interactions because, when coiled up, the cavity is hydrophobic while the outer surface is hydrophilic.[7] Amylose−lipid inclusion complexes have been extensively studied because of their valuable applications in food processing such as reducing the stickiness of starch, improving freeze−thaw stability and having an antistaling effect in bread and biscuits, due to reduced crystallization (retrogradation) of the amylopectin fraction in starch.[8−10] A better understanding of the inclusion complex formation and its optimization are essential not only for the food industry but also for the nonfood applications of starch.[11]

Numerous studies have been carried out on the influence of amylose−lipid complexes on the quality of food (e.g., prevention of staling,[12,13] digestibility,[14] and embrittlement[15]), its rheological properties,[16] and the physical properties of biodegradable starch-related materials.[17] Amylose−lipid inclusion complexes have been explored by differential scanning calorimetry (DSC), nuclear magnetic resonance spectroscopy (NMR) and X-ray diffraction analysis.[9,18−24] The results of these studies have been summarized in an excellent review by Tomasik and Schilling on inclusion complexes with amylose.[25] Despite these efforts, the dynamics of inclusion complex formation of amylose has yet to be investigated.[26] Furthermore, all research conducted so far utilized amylose or starch from natural sources, and in such systems it is impossible to obtain chains with a well-defined degree of polymerization and polydispersity.

Besides from natural sources, linear and branched polysaccharides can also be produced by using enzymatic polymerization;[27−30] this has the advantage that polysaccharide chain length with a very low polydispersity and degree of branching can be highly controlled.[27−31] Recently, linear and branched polysaccharide chains synthesized on different surfaces by enzymatic "grafting from" polymerization have been reported.[32−36] In the so-called "grafting from" approach, polymers are grown from initiators bound to surfaces, and this represents a superior alternative since the functionality, density, and thickness of the polymer brushes can be controlled with almost molecular precision. The resulting layer of amylose brushes attached to a solid support can be used as a simplified two-dimensional model system for studying the dynamics of amylose−lipid inclusion complex formation. A QCM consisting of a small α-quartz disk sandwiched between two gold

Received: July 24, 2013
Revised: September 14, 2013
Published: September 17, 2013

 © 2013 American Chemical Society

electrodes is considered as a commonly used technique. Since the resonance frequency of the quartz scales with the mass loaded on the crystal surface, mass changes at the nanogram level can be recorded. In addition, QCM with dissipation monitoring (QCMD) can provide information on the viscoelastic properties of adsorbed layers. QCM has already been widely used for studying the conformation of polymer brushes,[37,38] protein adsorption,[39] viscoelasticity of hydrogel thin films[40,41] and multilayer assembly of polyelectrolytes.[42] The surfaces of QCM sensors are easily modified with amylose brush via the "grafting from" polymerization mentioned above.

In the present work, we report a unique new approach to study the amylose-lipid system, which makes use of amylose brushes attached on surfaces and of the QCM-D technique. The well-defined amylose brushes were prepared on gold-covered surfaces of QCM sensors by a three-step synthetic pathway. Fourier transform infrared (FT-IR) spectroscopy, spectroscopic ellipsometry, single molecule force microscopy, and X-ray photoelectron spectroscopy (XPS) were used to characterize the amylose brushes in detail. The dynamics of the inclusion complex formation between amylose brushes and two fatty acids was investigated under various conditions including the effect of lipid concentration, layer thickness of amylose brushes, and lipid chain length with the help of the QCM-D immersed in the liquid phase.

EXPERIMENTAL SECTION

Chemicals and Materials. QCM sensors with gold coating were purchased from Q-sense. Double-sided polished silicon wafers were purchased from TOPSIL (Frederikssund, Denmark). Toluene was freshly purified in a SPS-800 Solvent Purification System (MBRAUN). α-D-Glucose-1-phosphate disodium salt hydrate (G-1-P, 97%), anhydrous ethylene glycol (99.8%), dimethyl sulfoxide (DMSO, 99.7%), cysteamine (98%), 3-aminopropyldimethyehtoxysilane (APDMES, 97%), rabbit muscle phosphorylase b (RMP b, 20 U/mg), DL-dithiothreitol (DTT, 99%), adenosine 5′-monophosphate (AMP, 97%), octanoic acid (C8, 99%), and myristic acid (C14, 95%) were purchased from Sigma-Aldrich and used as received. Maltoheptaonolacone was obtained according to the procedures reported in literature.[43,44]

Functionalization of the Gold Surfaces with Cysteamine. QCM sensors were soaked in the mixture of milli-Q water, hydrogen peroxide (30%), and ammonium hydroxide (5:1:1) at 75 °C for 30 min. Subsequently the sensors were thoroughly washed with milli-Q water and ultrasonicated in water 3 times. As a last cleaning step, the samples were treated in the UV-Ozone for 30 min. Then the QCM sensors were immersed in a 18 mM cysteamine solution in water to create a self-assembled monolayer on which the primer can be grafted. The reaction was carried out at room temperature in the dark overnight. After the reaction, the samples were rinsed with large amounts of milli Q water, ethanol, and acetone.

Si Wafers Amination with APDMES. The Si wafers were cut into small pieces of roughly 1 × 2 cm^2 and subjected to the following cleaning protocol: ultrasonic rinsing with ethanol (20 min), ethanol/dichloromethane 50/50 (20 min), and dichloromethane (20 min), and finally submersion in a Piranha solution (1:3 (v/v) 30% H_2O_2/concentrated H_2SO_4) at 75 °C for 1 h.

Following this chemical cleaning, the Si wafers were rinsed with plenty of milli-Q water and sonicated in methanol and toluene. To create the APDMES surface-termination, the samples were then immersed in an excess of 10 mM APDMES solution in fresh toluene in a shaking incubator at room temperature. After 5 h, the substrates were rinsed with toluene and placed in a Soxhlet apparatus with toluene for 24 h to remove the excess APDMES. Thereafter the samples were kept at 110 °C for 1 h to remove solvent residues and eventually bring the sol−gel reaction to completion.

Attachment of the Primer Maltoheptaonolactone to the Amino-Functionalized Surfaces. The amino-functionalized surfaces were immersed in a 10 mg mL^{-1} maltoheptaonolactone solution in ethylene glycol. The reaction was carried out at a temperature of 65 °C for 10 h in a shaking incubator. After the reaction, the samples were rinsed copiously with milli-Q water and subsequently ultrasonicated in milli-Q water and ethanol.

Synthesis of Amylose Brushes by Enzymatic Polymerization. Maltoheptaonolactone-functionalized surfaces were immersed in a TRIS buffer (pH 6.7, 0.1 M) solution containing G-1-P (250 mM), AMP (1.20 mM), DTT (1.36 mM), and RMP b (2.50 Uml^{-1}). The reaction was allowed to proceed for 4−11 days at 38 °C in a shaking incubator. Once the reaction was completed, the surfaces were abundantly rinsed with milli-Q water and sonicated in milli-Q water, DMSO, acetone, and methanol.

Instrumental and Characterization. FT-IR measurements were performed at a resolution of 3 cm^{-1} under vacuum on a Bruker 66 V/S FT-IR spectrometer equipped with a mid-infrared (MIR) deuterated triglycine sulfate (DTGS) detector. A sample shutter accessory was used for interleaved sample and background scanning. A clean double-sided polished silicon wafer was used as reference. Characterization of the amylose brush functionalized gold surfaces of QCM sensors was carried out by reflection adsorption infrared (RAIR) spectroscopy, using the same FT-IR spectrometer. An angle of incidence of 70° to the surface was used in the measurements on amylose-covered gold surfaces. A clean gold surface was also measured as background prior to the measurements.

Spectroscopic ellipsometry was performed on a variable-angle spectroscopic ellipsometer (VASE) VB-400 in the range of 400−1000 nm. The angle of incidence was varied between 74° and 76 ° in 1° steps. The software package WVASE32 was used to make a model consisting of different layers with characteristic values for the refractive indices. A Cauchy dispersion layer was used to determine the thickness of the cysteamine, maltoheptaonolactone and polysaccharide layers. The refractive index of maltoheptaonolactone and of the α-glucan brush was taken to be 1.336, that of cysteamine was 1.45.

Single molecule force spectroscopy measurements were performed with a PicoPlus 5500 microscope (Agilent Technologies, Inc.) on the amylose brushes grafted in the same way as described for the QCM sensor on flame annealed gold films on mica, prepared beforehand in a custom-made evaporator as described in the reference.[45] The cantilevers/tips were MLCT (Bruker, nominal spring constant 10 pN/nm) or OBL (Bruker, nominal spring constant 30 pN/nm). Unspecific interactions (physisorption) between the atomic force microscope (AFM) tip and the sample molecules were used to trap the chains and to stretch them. The measurements were performed in DMSO. The contour length of the stretched amylose chains was estimated by fitting the worm-like-chain model to the experimental curves. The analysis was performed with a homemade routine developed in the Igor environment.

XPS spectra were recorded on a Surface Science Instruments SSX-100 photoelectron spectrometer with a monochromatic AlK_α X-ray source ($h\nu$ = 1486.6 eV). For the XPS measurements, evaporated gold films supported on glass and prepared as described in the ref 46, were used as substrates. The energy resolution was set to 1.16 eV to minimize the measuring time. The photoelectron takeoff angle was 37° with respect to the surface normal. All binding energies were referenced to the Au4$f_{7/2}$ core level signal of the substrate. Spectral analysis was carried out with the WinSpec program developed at the University of Namur, Belgium. Three different points on each sample were analyzed to check for homogeneity. The photoemission peak intensities of each element, used to estimate the amount of each species on the surface, were normalized by the sensitivity factors of each element tabulated for the spectrometer used.

The dynamics of complex formation between amylose brushes on gold and fatty acids was characterized with a Q-sense E4 quartz crystal microbalance with dissipation monitoring (QCM-D, QSENSE, Västra Frölunda, Sweden) in a liquid medium at 25 °C. The QCM sensor was an AT-cut quartz crystal with 10 mm diameter gold electrode (QSX301) with a fundamental frequency f_0 of 5 MHz. All QCM-D

Scheme 1. Synthesis of Amylose Brushes on Si and Au Surfaces via a Three Step Synthetic Pathway

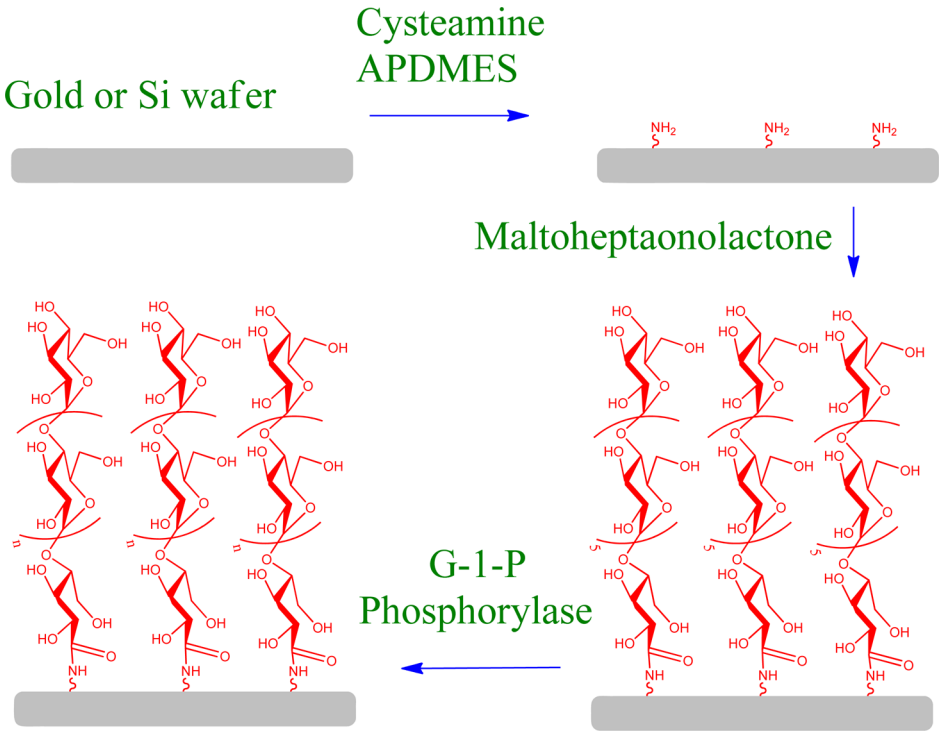

measurements were performed under flowing condition with a flow rate of 50 μL/min. The Au-coated QCM sensors were modified with amylose brushes ex situ following the three-step synthetic pathway described above. After enzymatic polymerization, the amylose brush-covered QCM sensors were transferred to a standard Q-sense flow module (QFM 401) and equilibrated in solvents including water, DMSO, and a 9:1 mixture of DMSO and water, for 1 h at a constant temperature of 25 °C for each entire experiment. The resonance behavior of the amylose brush-coated QCM sensors in solvents was first recorded as the baseline. Then the fatty acid solution at certain concentration was introduced to the flow module chamber and also kept at a constant flow rate of 50 μL/min.

The complex formation between amylose and fatty acids was detected by the mass change on the sensor surface. The QCM signals including frequency shifts (Δf) and dissipation shifts (ΔD) were acquired at the third (15 MHz), fifth (25 MHz) and seventh (35 MHz) harmonic. The standard way to accurately determine the adsorbed mass on the soft amylose layer in the liquid, is to model this mass with a Voigt model with the help of the Q-tool software and requires one to determine the frequency and dissipation shift induced by the amylose layer alone before the dynamics study. This approach is, however, not feasible in our case because it entails measuring first the unmodified sensor in air and liquid to retrieve the frequency shift and dissipation data for the bare surface, then to prepare the amylose brushes on the surface ex situ and thereafter measure again the amylose brush-modified sensor in air and in the liquid. Since this implies mounting and demounting the sensor and since placing the sensor differently onto the O-ring each time gives different frequency changes, the error introduced would be unreasonably large. For this reason, our QCM-D measurements were started directly with the amylose brush-modified QCM sensor surfaces in the liquid. The frequency and dissipation responses in the pure solvent were recorded as the baseline, and then both the frequency shift and the dissipation shift caused by the inclusion complex formation were further monitored after the addition of the fatty acid solution. The adsorbed mass change was estimated from the Sauerbrey equation:[47]

$$\Delta m = -c\Delta f_n/n \quad (2)$$

where Δf_n is the frequency shift, Δm is the areal mass density of the adsorbed fatty acids, c (17.7 ng cm^{-2} Hz^{-1}) is mass-sensitivity constant and n is the harmonic number (3, 5, 7). Although the Sauerbrey equation is only valid for rigid homogeneous thin films, the mass values estimated in this fashion are still useful for following semiquantitatively the dynamics of the fatty acid adsorption on the amylose brushes.

RESULTS AND DISCUSSIONS

Synthesis and Characterization of Amylose Brushes on Gold Surfaces and Si Wafers. A series of samples with amylose brushes with controlled thickness were synthesized following the three-step synthetic pathway on the gold electrodes of QCM sensors, on Au/glass slides and on Si wafers. Scheme 1 shows the three steps of the reaction, namely, the amino-functionalization of the surfaces with cysteamine or APDMES, which is followed by the grafting of the maltoheptaonolactone primer onto the amino functionalized surfaces, and finally enzymatic polymerization of G-1-P catalyzed by RMP b. Details about the synthesis and characterization of maltoheptaonolactone used in this experiment can be found in the Supporting Information (Figures S1 and S2).

From the ellipsometric measurements, the thickness of cysteamine on gold surfaces was found to be 0.56 ± 0.20 nm, which is in good agreement with literature data.[48] The enzymatic polymerization of G-1-P catalyzed by phosphorylase needs a primer—a short oligosaccharide containing at least 3 glucose units. In our experiments, the oxidized maltoheptaose, maltoheptaonolactone containing seven glucose units was used and coupled to the amino-functionalized surfaces. The thickness of the maltoheptaonolactone on the amino-functionalized gold surface was again determined by ellipsometry to amount to 1.03 ± 0.15 nm . After attachment of maltoheptaonolactone onto the surfaces, enzymatic "grafting from" polymerization of G-1-P was performed with RMP b as

dx.doi.org/10.1021/bm4010904 | Biomacromolecules 2013, 14, 3713−3722

catalyst. The desired thickness of amylose brushes can be tuned in the range from 4 to 20 nm by setting the reaction time between 4 to 11 days, as shown in Figure 1.

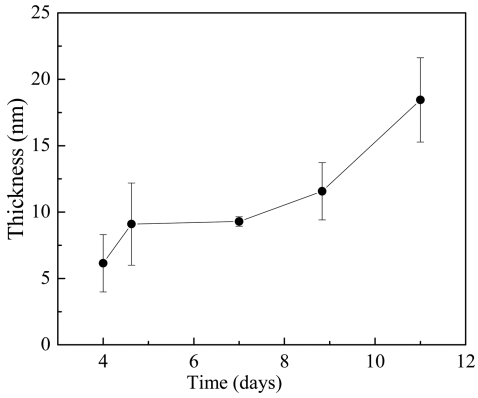

Figure 1. Thickness of amylose brush layers on gold surfaces (as determined from ellipsometric measurements) versus reaction time.

As expected, the thickness of amylose brushes on gold surfaces increases as the reaction time increases. This precise thickness control of amylose brush layers on gold surfaces provides an ideal two-dimensional platform with a well-defined degree of polymerization (*vide infra*), which is ideal for studying the inclusion complex formation between amylose and fatty acids.

Figure 2 shows the FT-IR spectra of the APDMES-, maltoheptaonolactone-, and amylose-functionalized Si wafers

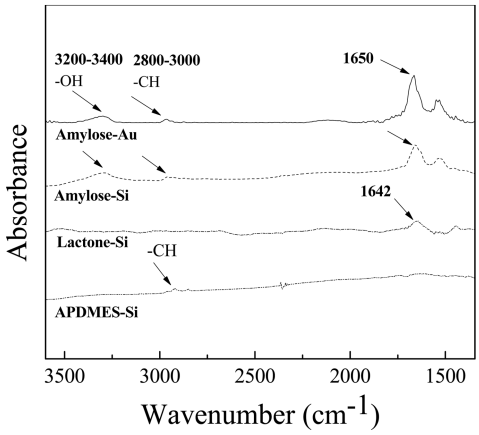

Figure 2. FT-IR spectra of the APDMES-, maltoheptaonolactone-, and amylose brush-functionalized Si wafers and RAIR spectrum of amylose brush-functionalized gold surfaces.

during the three steps and the RAIR spectrum of an amylose brush-functionalized gold surface of a QCM sensor. Here a clean double-sided polished Si wafer and a clean gold QCM sensor were used as references, respectively. The FT-IR spectrum of the APDMES-functionalized Si surface shows two weak absorption bands at 2800−3000 cm^{-1}, assigned as due to CH and CH_2 stretching modes. The maltoheptaonolactone-functionalized Si wafer exhibits the characteristic peak of amide group at 1642 cm^{-1} arising from the formation of an amide bond between lactone and amino groups on surfaces. In the FT-IR spectrum of the amylose-functionalized Si wafer, the characteristic absorption of sugar hydroxyl groups is distinguished between 3200 cm^{-1} and 3400 cm^{-1}, which is also confirmed in the RAIR spectrum of the amylose-functionalized gold surfaces. Hence both FT-IR and ellipsometry measurements confirm that the amylose brushes were grown from the Si wafers and gold surfaces.

Verifying the layer thickness and demonstrating the presence of the expected chemical groups is not sufficient to characterize the amylose brushes, as we also need to determine the single chain length of amylose brushes attached onto the surfaces. One approach would be to use a cleavable spacer between the support and the maltoheptaonolactone primer, so that the polymer can be separated from the surface and be analyzed by GPC or light scattering techniques. A more direct approach is to determine the chain length of the amylose brushes by single molecule force spectroscopy. In fact, recently such measurements have been utilized to estimate the length of the stretched molecules.[49] Here amylose brush samples on gold surfaces prepared following the identical protocol employed for the functionalization of the QCM sensor were chosen for the measurements. For a sample where the enzymatic polymerization was carried out for 11 days with the enzymatic activity 2.5 uml^{-1} an average brush length of about 16.2 nm was obtained. The contour lengths of the stretched amylose chains gold surfaces were evaluated by fitting the worm-like-chain model to the experimental curves.[50] The distribution of the evaluated contour lengths is reported in Figure 3.

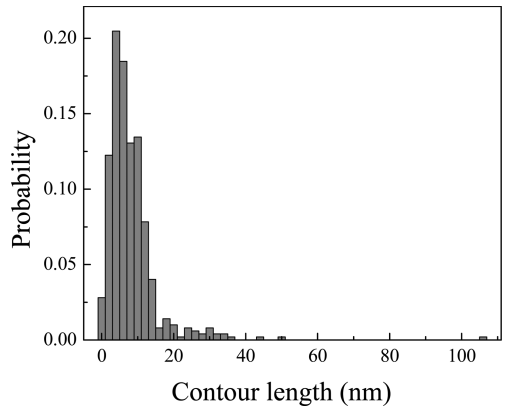

Figure 3. Histogram of the contour lengths of the stretched amylose segments estimated by fitting the worm-like-chain model to the single molecule force spectroscopy experimental curves for amylose brushes prepared on a flame-annealed gold substrate.

It is important to note that in these force spectroscopy measurements the tip picks up the chain at a random position along its length because the interaction between tip and chain is unspecific. Considering that a minimum segment length of about 10 nm is required for a stable physisorption on the tip[51] and that the distribution of the stretched segments is centered on 8−9 nm (Figure 3), we can estimate a total chain length of about 20 nm. This is comparable to the layer thickness (16.2 nm) of amylose brushes on the gold surface of the QCM sensors.

The grafting density of lactone on gold surfaces is calculated according to eq 2:[35,52]

$$\sigma = L\rho N_A/M_n \quad (1)$$

The layer thickness of lactone is L = 1.03 nm, the density of lactone ρ = 1.0386 g mL^{-1} (assuming the density of the lactone

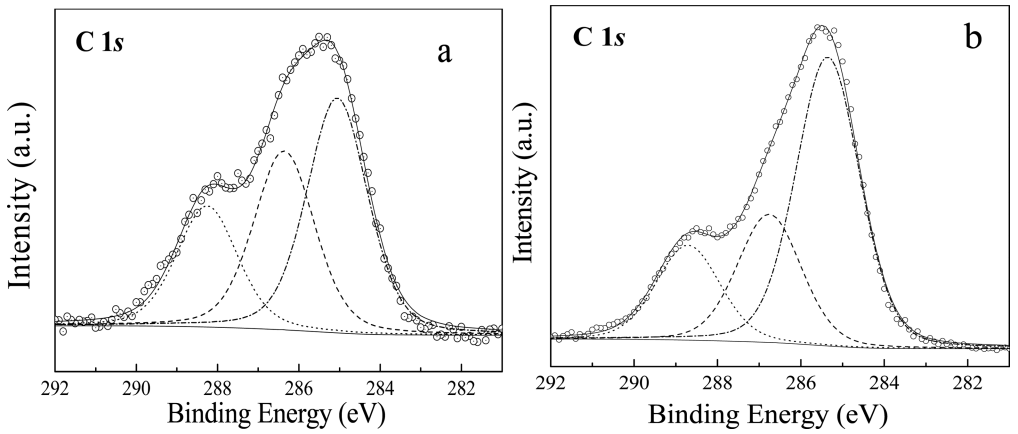

Figure 4. High-resolution photoemission spectra (scattered symbols) and fit of C 1*s* core level region of amylose brushes grafted on a gold surface before (a) and after (b) exposure to octanoic acid (C8).

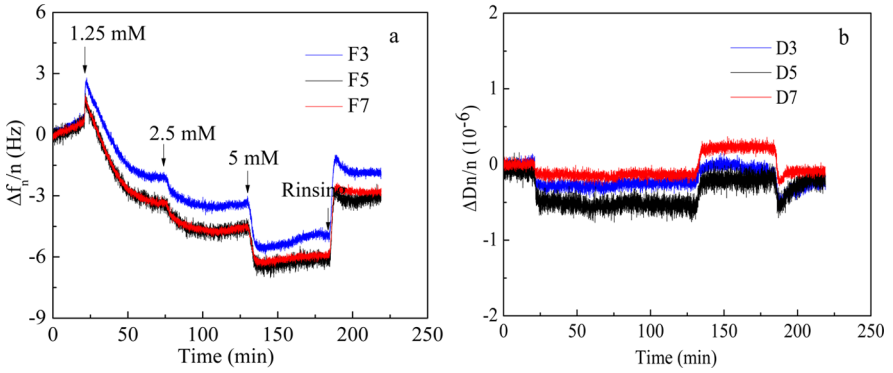

Figure 5. Frequency shift ($\Delta f_n/n$) and dissipation shift ($\Delta D_n/n$) at different harmonics (harmonic number indicated) as a function of time for the adsorption of octanoic acid (C8) at successively increased concentration (1.25 mM, 2.5 mM, 5 mM) onto amylose brush modified QCM sensor surfaces during the same adsorption run (layer thickness 4.2 nm).

is the same as for maltoheptaose), and its molecular weight M_n = 1152 g mol^{-1}, and N_A is the Avogadro constant; hence a grafting density of lactone on gold surfaces of 0.6 nm^{-2} is found. This value was lower than that of maltoheptaose prepared on Si wafers (1.90 nm^{-2}), reported by van der Vlist.[35] The difference can be explained by the difference in reaction conditions, namely, the Si substrate and the chemicals employed. The amount of primer maltoheptaonolactone per square nanometer determines the maximum grafting density of amylose brushes on the gold surfaces. If 100% of the maltoheptaonolactone molecules act as primer recognition sites for phosphrorylase, the grafting density of linear amylose brushes grafted from the gold surface can be estimated at 0.6 nm^{-2}. This value should be the same for all samples prepared on gold surfaces because the different reaction times only determine the length but not the number of chains, which is instead defined by the density of primer molecules on the surface.[35]

Before studying the dynamics of the inclusion complex formation, XPS was employed to examine the chemical composition of amylose brushes on gold before and after complexation with the typical fatty acids to verify that the latter adsorb.

The high-resolution carbon 1*s* core level XPS spectra are presented in Figure 4. The spectrum of the as-prepared amylose brushes on gold (Figure 4a) can be fitted with three components: the highest binding energy component, recorded at 288.2 eV, is attributed to the O−C−O bonds and accounts for 22% of the total carbon intensity; the two other components originate from C−OH at 286.3 eV (34% of the overall C intensity) and at 285.0 eV (44% of the overall carbon intensity), respectively. The split of the C−OH signal results from differences in hydrogen bonding along the amylose helix as explained in detail for amylose brushes prepared with maltoheptaose as primer.[36] This C1*s* XPS spectrum testifies together with the data from FT-IR spectroscopy, spectroscopic ellipsometry, and single molecule force spectroscopy to the synthesis of amylose brushes on gold surfaces.

The self-assembled layer of amylose brushes on gold was immersed in a 5 mM octanoic acid (C8) solution in water overnight. After the removal of the uncomplexed C8, the sample was again examined by XPS, and the C1*s* core level region of the XPS spectrum is shown in Figure 4b. The spectrum was also fitted employing three components at binding energies of 288.3, 286.4, and 285.0 eV. However, compared with the corresponding XPS spectrum of pure amylose brushes on gold, the intensity of the peak at 285.0 eV was found significantly increased (55% of the overall carbon area) mainly due to the additional contribution of the aliphatic chains (−CH_2−)[53] of the introduced C8 fatty acid. This result confirms the adsorption of octanoic acid onto the amylose brushes and therefore hints to the inclusion complex formation between amylose brushes and fatty acids on gold, which was studied in the following QCM-D measurements.

The Dynamics of Complex Formation between Amylose Brushes on Gold and Fatty Acids by QCM-D.

dx.doi.org/10.1021/bm4010904 | *Biomacromolecules* 2013, 14, 3713−3722

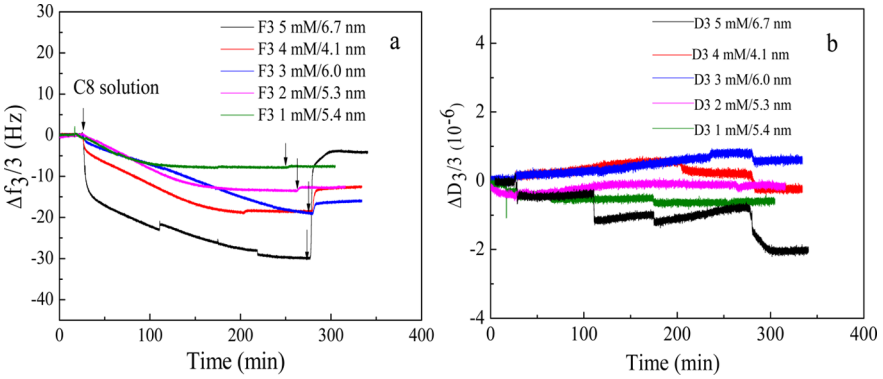

Figure 6. Frequency shifts ($\Delta f_3/3$) and dissipation shifts ($\Delta D_3/3$) at the third harmonic as a function of time, recorded for amylose brush-modified QCM sensors exposed to C8 aqueous solutions with different concentrations. The legend lists the concentration of C8 and the thickness (determined by ellipsometry) of the as-prepared amylose brushes used in the various experiments.

Figure 5 shows the frequency and dissipation responses for the adsorption of the short chain octanoic acid (C8) onto the amylose brush-modified gold surfaces of QCM sensors in water. The layer of amylose brushes (layer thickness 4.2 nm) was allowed to stabilize in water before it was exposed to the C8 solution. When the 1.25 mM C8 aqueous solution is introduced, the frequency shift decreased, indicating the adsorption of lipid molecules onto the amylose brush-covered sensor surfaces or complex formation. When solutions with higher lipid concentrations, namely, 2.5 mM and 5 mM, were successively introduced, larger frequency shifts were observed, pointing to adsorption of more C8. Note that the solubility of C8 in water is about 4.7 mM (0.068 g/100 mL) at 25 °C. After rinsing the saturated surfaces with water, the physically adsorbed C8 molecules were washed away, and the complexation between amylose brushes and C8 led to the final frequency shift of about 2.6 Hz at the third harmonic.

The dissipation shift recorded by QCM-D can provide additional information on the structures and viscoelastic properties of thin layers deposited on the quartz crystal but in our case also reveals complex formation. A soft film adsorbed on the sensor surface is deformed during the oscillation of quartz crystal, and this leads to higher dissipation. By contrast, a rigid and compact thin film on the sensor surface gives low dissipation. As seen in the lower part of Figure 5, the dissipation shift at the third, fifth, and seventh harmonic first decreased slightly when the first C8 solution was introduced and then reached a stable negative value; when more C8 molecules adsorbed after successive introduction of the 2.5 mM and 5 mM solutions, the dissipation shift increased and finally reached the baseline again after rinsing with water. It was also found that these curves were not completely spreading in Figure 5, indicating that this amylose brush layer is a little rigid during the C8 adsorption. In normal adsorption experiments, ΔD typically increases with adsorption due to the formation of loose and elongated structures. In our measurements, the dissipation shift instead decreased after adsorption of C8 molecules and this indicates that the C8 molecules penetrated into the amylose hydrophobic cavities forming an inclusion complex, and thereby made this layer slightly stiffer and more compact. On the other hand, the slight increase in dissipation shift after a higher concentration of C8 solution (5 mM) was added specifies that the C8 molecules also adsorbed on the surface, in addition to forming complexes with the amylose brushes. Upon rinsing, it is likely that some or all of C8 molecules that had been adsorbed on top of amylose brushes were carried away, and that this is the reason for the decrease in ΔD.

The overall mass of C8 molecules complexed with the amylose brushes after rinsing, when the net frequency shift was about 2.6 Hz at the third harmonic (Figure 5), was estimated at 46.0 ng/cm^2 by the Sauerbrey equation. This translates into an areal density of C8 molecules of 1.9 nm^{-2} for a layer of amylose brushes with a thickness of about 4.2 nm. The C8 density was therefore larger than that of amylose brushes (0.6 nm^{-2}) obtained above. That means each amylose helix includes approximately three C8 molecules.

We also studied in detail how the dynamics of lipid C8 adsorption on the amylose brush depends on the concentration of the C8 aqueous solution. Figure 6 shows frequency and dissipation responses of amylose brush-modified QCM sensors in individual C8 aqueous solutions with different concentration, i.e., 1 mM, 2 mM, 3 mM, 4 mM, and 5 mM. The legend lists the corresponding amylose layer thicknesses. As mentioned in the synthesis part, amylose brushes with different thicknesses can be obtained by varying the reaction time. In this experiment, within a thickness range of 4.1 to 6.7 nm, the C8 concentration was considered to be the only parameter adjusted for studying the C8 adsorption on amylose brush-covered surfaces. In all cases, the frequency shift at the third harmonic decreased when exposing the amylose brushes to the C8 solutions. The sensors exhibited a higher frequency response in C8 aqueous solution with higher concentration, indicating that a higher amount of molecules were adsorbed. However, the net frequency shift obtained after rinsing with water was much smaller than that at saturation and increased when the concentration increased from 1 mM to 3 mM, but decreased when the concentration further increased from 3 mM to 5 mM. During the measurements, it was also found that there were several slight steps on the adsorption curves probably due to the temperature fluctuations or disturbances induced by the peristaltic pump. The maximum adsorption was found for a concentration of 3 mM. While the increase on going from 1 mM to 3 mM can be explained simply by the larger number of molecules available for complex formation, the lower value of the frequency shift after rinsing for the 5 mM solution results from the solubility of C8 in water, which is 4.7 mM at 25 °C. In fact, this solubility value implies that at the high concentration of 5 mM used in our measurements C8 micelles form in solution due to the hydrophobic nature of aliphatic part, and these micelles can physically adsorb onto the amylose brush. Hence in this case, the water can rinse away

dx.doi.org/10.1021/bm4010904 | Biomacromolecules 2013, 14, 3713−3722

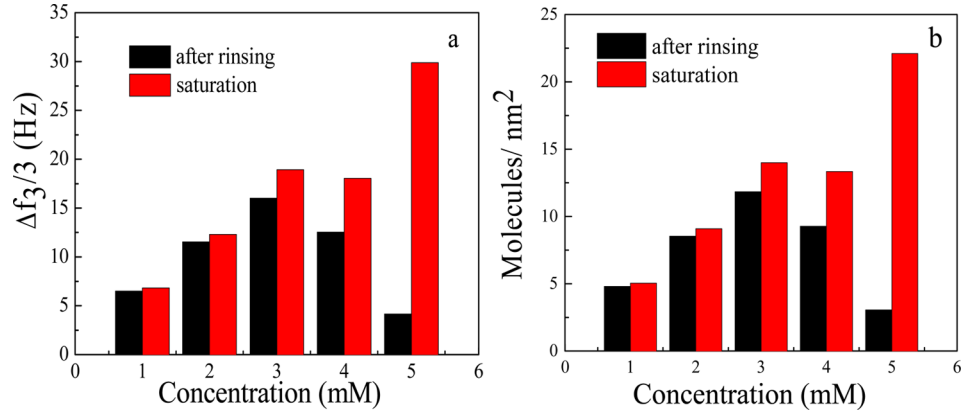

Figure 7. Frequency shifts ($\Delta f_3/3$) (a) and areal densities of adsorbed C8 molecules (b) at saturation and after rinsing with water for various concentrations of C8 in water.

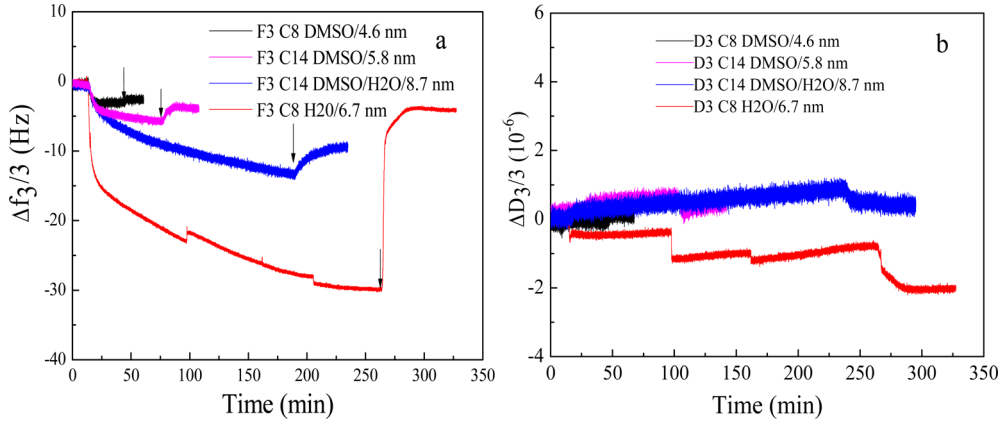

Figure 8. Frequency shift ($\Delta f_3/3$) and dissipation shift ($\Delta D_3/3$) as a function of time for adsorption of octanoic acid (C8) and myristic acid (C14) onto amylose brush-modified surfaces in liquid from at 5 mM solutions. The legend lists the solvent and the thickness (determined by ellipsometry) of the as-prepared amylose brushes used in the various experiments. The arrows indicate when the layer was rinsed with pure solvent.

most of the adsorbed lipid molecules from the brush surfaces, and the final frequency shift upon rinsing results much smaller than the value at saturation. This interpretation is also supported by the dissipation shift data in Figure 6. When the concentration of C8 in water was 5 mM, the dissipation shift always decreased to more negative values after adding the C8 solution. As already mentioned, this is explained by the formation of inclusion complexes between amylose helix and C8 molecules resulting in a more rigid structure. At the same time, it is possible that C8 molecules formed a compact layer on the top of the amylose layer due to the high concentration of C8. Once water was added to rinse the surfaces, the $\Delta f_3/3$ increased while $\Delta D_3/3$ decreased greatly because the lipid layer was washed away, which resulted in more compact and rigid structures.

Based on the Sauerbrey equation, the approximate areal density of C8 molecules was calculated as reported in the Figure 7. The maximum amount of adsorbed C8 was about 11 molecules/nm^2 when the adsorption proceeds from a 3 mM solution. Such a high value of the areal density could be interpreted as implying that about 18 molecules were included into one amylose helix due to the hydrophobic interactions. However, this value cannot be considered an accurate determination because the dissipation shift upon rinsing was about 0.6×10^{-6} (greater than 0), which means the amylose layer became less dense and elongated after the adsorption of C8 molecules. Nevertheless, the thickness of amylose brushes was about 6 nm, which allows more than one C8 molecule to enter the hydrophobic cavity of the amylose helix. When a 6.7 nm thick amylose layer was exposed to a 5 mM solution of C8 molecules, the areal density after rinsing implies that about 5 molecules were included into one amylose helix. Compared with 3 C8 molecule per amylose obtained at successively increased concentration (1.25, 2.5, 5 mM) above (Figure 5), it is reasonable that thicker amylose brushes can include more C8 molecules.

To gain more insight into the inclusion complex formation between amylose brushes and lipids, we also examined a lipid with a longer chain, namely, myristic acid (C14). To compare C8 and C14, the experiments were not performed in water, where C14's extremely poor solubility precludes the experiments, but in DMSO and in a 9:1 mixture of DMSO/H_2O. As for the experiments in water, the amylose brush-modified QCM sensors were let to stabilize in DMSO and DMSO/H_2O, respectively, before they were exposed to myristic acid (C14) solution. The frequency and dissipation shifts recorded before and during exposure to C8 and C14 and subsequent rinsing with pure solvent are shown in Figure 8. One immediately sees that the adsorption of both C8 and C14 onto the amylose layer depends strongly on the solvent. If one compares the frequency shift curves for C8 in water and in DMSO, one notes that the uptake in DMSO is much lower and saturates much faster than

dx.doi.org/10.1021/bm4010904 | Biomacromolecules 2013, 14, 3713−3722

in water. The same is also seen comparing the adsorption of C14 in DMSO and in the DMSO/H_2O mixture. One reason for these differences is that the structure of the amylose brushes changes depending on the solvent. In fact, Chetham and Tao[54] reported that the amylose conformation in DMSO/water mixtures changes from a tight helix in pure DMSO to a looser helix and finally to a random coil when the water content reaches 66%. Obviously, if a helical structure is already formed, the inclusion complex formation can proceed faster. On the other hand, DMSO can also form complexes with amylose,[55,56] which possibly explains the low uptake of C8 and C14 if the lipids cannot displace DMSO. A further reason for the different dynamics is that water molecules can penetrate into the inside of amylose cavity besides interacting with hydroxyl groups on the surfaces of amylose.[57] Additionally, hydrogen bonds between amylose and water,[57] which have to be broken to form the inclusion complex, can also slow down the process. These reasons explain why it takes longer to reach the adsorption equilibrium in an aqueous solution. This picture is confirmed and refined if one considers the dissipation shifts also reported in Figure 8. $\Delta D_3/3$ increased to more positive values with the adsorption of C8 and C14 on the amylose layer when performed in DMSO and DMSO/H_2O. After rinsing with DMSO and DMSO/H_2O, respectively, the dissipation shifts decreased slightly but remained at more positive values than before the adsorption experiment was started. This is different from the formation of amylose-C8 complexes in water where a lower $\Delta D_3/3$ value is reached in the end, and leads to the conclusion that the complexes formed in DMSO and DMSO/H_2O must have less dense and elongated structures. Again coming back to the structure determination of amylose brushes by Chetham and Tao and to the calculations by Krüger and Fels, the following interpretation of the dissipation shifts emerges: in water, the as-prepared amylose brushes are coiled and highly hydrated due to the interactions between water molecules and all hydroxyl groups in the amylose chains. The soft layer becomes more rigid and compact after complexation, which explains the decreased dissipation shifts. In DMSO instead, the as-prepared amylose brushes form a more rigid structure because helices are formed and stabilized by the DMSO in the cavity.[55,56] These rigid structures become less dense and elongated (less negative dissipation shift) after the complexation with fatty acids.

As for the experiments concerning C8 adsorption in water, the Sauerbrey equation was employed to determine the areal density of lipid molecules for adsorption in DMSO. For C8 and C14 we found that 2.5 lipid molecules are included in each amylose hydrophobic cavity for 4.6 and 5.8 nm thick amylose brush layers.

Besides the influence of the type of solvent and of the solution concentration, we also studied the effect of the amylose chain length on the dynamics of the complex formation between amylose brushes on gold and fatty acids. Figure 9 shows the frequency response as a function of time for the adsorption of myristic acid (C14) from a 5 mM DMSO solution onto amylose brushes with different thickness ranging from 4.4 to 14.0 nm. One sees that the frequency shift at saturation increases with the thickness of amylose brushes and hence deduces that the adsorption scales with the chain length, in agreement with literature data[58] reporting that longer amylose chains can complex more lipid molecules. After rinsing with DMSO, there was still a certain amount of C14 molecules that remained in the amylose hydrophobic cavities.

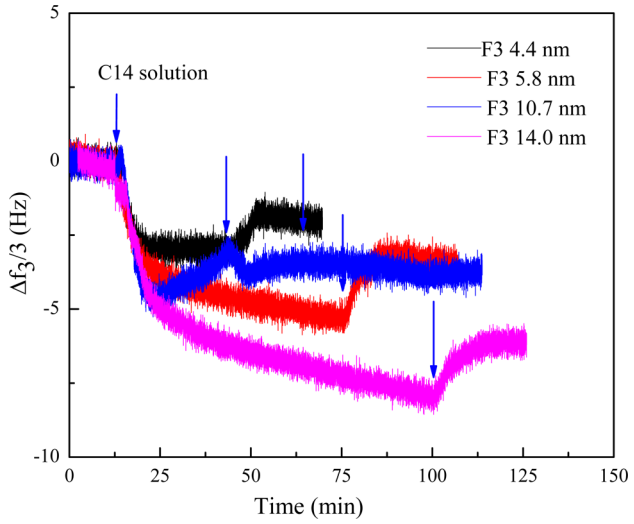

Figure 9. Frequency shifts ($\Delta f_3/3$) as a function of time for adsorption of myristic acid (C14) onto amylose brush-modified surfaces from a 5 mM solution in DMSO. The legend lists the thickness (determined by ellipsometry) of the as-prepared amylose brushes used in the various experiments.

Figure 10a illustrates the frequency shifts when the adsorption saturates and after rinsing for different thickness of the amylose brushes. We referred again to the Sauerbrey equation to calculate the areal density of C14 molecules in complexes formed in DMSO; the results are listed in the Figure 10b. When the amylose chains were relatively short (thickness of the layer 4.4 nm), only 1.5 C14 molecules per amylose were complexed on the surface.

Compared with 2.5 C8 molecules per amylose chain obtained for a similarly thick layer in DMSO, the amount of adsorbed C14 molecules was much smaller due to the longer chain length of C14. When the thickness of the amylose layer was 14.0 nm, almost 5 C14 molecules were found to be included in each amylose helix.

CONCLUSIONS

Amylose brushes were prepared on the gold surfaces by the "grafting from" enzymatic polymerization of Glucose-1-phosphate with RMP b as catalyst. FT-IR spectra, Ellipsometry, and XPS measurements confirmed the growth of the amylose brushes via a three-step synthetic pathway, including the amino-functionalization, attachment of the primer, and finally enzymatic polymerization. Single force microscopy allowed to determine the length of the amylose chain, which is comparable to the layer thickness of the amylose brush layer. This two-dimensional amylose brush platform is an ideal system for detecting the inclusion complex formation with lipids by tuning the thickness of amylose brushes using different reaction times.

The dynamics of inclusion complex formation between amylose and fatty acids (C8 and C14) in different liquids, namely water, DMSO, and a 9:1 DMSO/H_2O mixture, was investigated using a quartz crystal microbalance with dissipation monitoring. When the experiments were performed in water, in the same thickness range of amylose brushes on gold, more C8 molecules were included inside the amylose helix when the C8 concentration in the water increased from 1 mM to 3 mM, but a higher C8 concentration (5 mM) led to C8 micelles in the water and less complexes formed on the surface. Solvent effects on the inclusion complex formation were investigated, and the

dx.doi.org/10.1021/bm4010904 | Biomacromolecules 2013, 14, 3713−3722

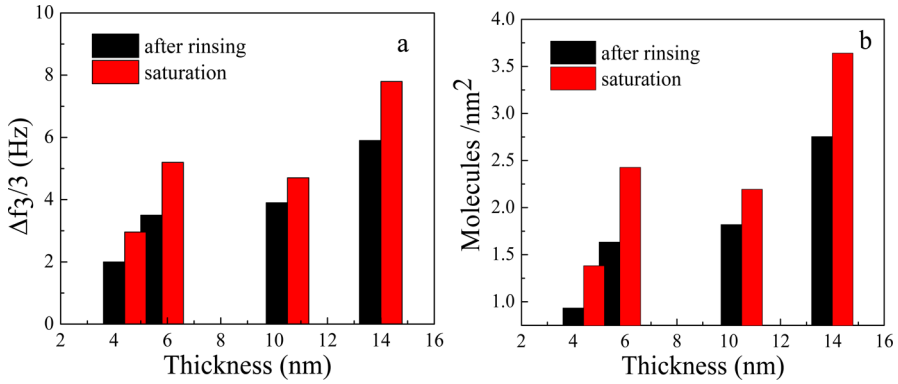

Figure 10. The frequency shifts ($\Delta f_3/3$) (a) and the areal density of C14 (b) at saturation (red) and after rinsing (black) as a function of the thickness of the amylose brushes on the surface.

complex formation was found to proceed faster in DMSO than in water, but less complexes were formed. Both effects were explained by the structure of the as-prepared layer of amylose brushes, coiled up in water, helical, and complexed with DMSO in the other cases. Finally, with increasing the amylose brush thickness, the adsorption process becomes slower but more molecules are complexed.

■ ASSOCIATED CONTENT

Ⓢ Supporting Information

Synthesis and characterization of maltoheptaonolactone. This information is available free of charge via the Internet at http://pubs.acs.org.

■ AUTHOR INFORMATION

Corresponding Author

*E-mail: p.rudolf@rug.nl and k.u.loos@rug.nl.

Notes

The authors declare no competing financial interest.

■ ACKNOWLEDGMENTS

Financial support of this research by the Foundation for Fundamental research on Matter (FOM) programme 'Bio(-related) materials' under Project Number 08BRM12 is gratefully acknowledged. The authors thank J. Wikström and A. Oom from Biolin Scientific for useful discussions and for their advice regarding the QCM-D data analysis.

■ REFERENCES

(1) Stein, R. S.; Rundle, R. E. *J. Chem. Phys.* **1948**, *16*, 195−207.
(2) Nimz, O.; Geßler, K.; Uson, I.; Laettig, S.; Welfle, H.; Sheldrick, G. M.; Saenger, W. *Carbohydr. Res.* **2003**, *338*, 977−986.
(3) Zabar, S.; Lesmes, U.; Katz, I.; Shimoni, E.; Bianco-Peled, H. *Food Hydrocolloids* **2009**, *23*, 1918−1925.
(4) Nishiyama, Y.; Mazeau, K.; Morin, M.; Cardoso, M. B.; Chanzy, H.; Putaux, J.-L. *Macromolecules* **2010**, *43*, 8628−8636.
(5) Kaneko, Y.; Saito, Y.; Nakaya, A.; Kadokawa, J.-i.; Tagaya, H. *Macromolecules* **2008**, *41*, 5665−5670.
(6) Rachmawati, R.; Woortman, A. J. J.; Loos, K. *Biomacromolecules* **2013**, *14*, 575−583.
(7) Immel, S.; Lichtenthaler, F. W. *Starch - Stärke* **2000**, *52*, 1−8.
(8) Gudmundsson, M. *Carbohydr. Polym.* **1992**, *17*, 299−304.
(9) Gudmundsson, M. *Thermochim. Acta* **1994**, *246*, 329−341.
(10) Salman, H.; Copeland, L. *Cereal Chem.* **2007**, *84*, 600−606.
(11) Raphaelides, S. N.; Dimitreli, G.; Exarhopoulos, S.; Mintzas, D.; Lykidou, A. *Carbohydr. Polym.* **2012**, *88*, 282−289.
(12) Farahnaky, A.; Majzoobi, M. *Int. J. Food Prop.* **2008**, *11*, 186−195.
(13) Purhagen, J. K.; Sjoeoe, M. E.; Eliasson, A.-C. *Eur. Food Res. Technol.* **2012**, *235*, 265−276.
(14) Putseys, J. A.; Lamberts, L.; Delcour, J. A. *J. Cereal Sci.* **2010**, *51*, 238−247.
(15) Shogren, R. L. *Carbohydr. Polym.* **1992**, *19*, 83−90.
(16) Singh, J.; Singh, N.; Saxena, S. K. *J. Food Eng.* **2002**, *52*, 9−16.
(17) Schmidt, V. C. R.; Porto, L. M.; Laurindo, J. B.; Menegalli, F. C. *Ind. Crops Prod.* **2013**, *41*, 227−234.
(18) Eliasson, A.-C. *Thermochim. Acta* **1994**, *246*, 343−356.
(19) Nuessli, J.; Sigg, B.; Conde-Petit, B.; Escher, F. *Food Hydrocolloids* **1997**, *11*, 27−34.
(20) Tufvesson, F.; Eliasson, A. C. *Carbohydr. Polym.* **2000**, *43*, 359−365.
(21) Tufvesson, F.; Wahlgren, M.; Eliasson, A.-C. *Starch - Stärke* **2003**, *55*, 138−149.
(22) Tufvesson, F.; Wahlgren, M.; Eliasson, A.-C. *Starch - Stärke* **2003**, *55*, 61−71.
(23) Abu-Hardan, M. O.; Hill, S. E.; Farhat, I. A. *Starch - Stärke* **2007**, *59*, 217−223.
(24) Kwasniewska-Karolak, I.; Nebesny, E.; Rosicka-Kaczmarek, J. *Food Sci. Technol. Int.* **2008**, *14*, 29−37.
(25) Tomasik, P.; Schilling, C. H.; Derek, H. *Adv. Carbohydr. Chem. Biochem.* **1998**, *53*, 345−426.
(26) Jovanovich, G.; Añón, M. C. *Biopolymers* **1999**, *49*, 81−89.
(27) Cori, G. T.; Cori, C. F. *J. Biol. Chem.* **1940**, *135*, 733−756.
(28) Husemann, E.; Burchard, W.; Pfannemüller, B. *Starch - Stärke* **1964**, *16*, 143−150.
(29) Ciric, J.; Oostland, J.; de Vries, J. W.; Woortman, A. J. J.; Loos, K. *Anal. Chem.* **2012**, *84*, 10463−10470.
(30) Ciric, J.; Loos, K. *Carbohydr. Polym.* **2013**, *93*, 31−37.
(31) Loos, K. *Biocatalysis in Polymer Chemistry*; Wiley-VCH: Weinheim, Germany, 2010.
(32) Loos, K.; von Braunmühl, V.; Stadler, R.; Landfester, K.; Spiess, H. W. *Macromol. Rapid Commun.* **1997**, *18*, 927−938.
(33) Breitinger, H.-G. *Tetrahedron Lett.* **2002**, *43*, 6127−6131.
(34) van der Vlist, J.; Palomo Reixach, M.; van der Maarel, M.; Dijkhuizen, L.; Schouten, A. J.; Loos, K. *Macromol. Rapid Commun.* **2008**, *29*, 1293−1297.
(35) van der Vlist, J.; Schönen, I.; Loos, K. *Biomacromolecules* **2011**, *12*, 3728−3732.
(36) Mazzocchett, L.; Tsoufis, T.; Svaldo-Lanero, T.; Duwez, A.-S.; Rudolf, P.; Loos, K. *Macromol. Biosci.* **2013**, DOI: 10.1002/mabi201300273.
(37) Fu, L.; Chen, X.; He, J.; Xiong, C.; Ma, H. *Langmuir* **2008**, *24*, 6100−6106.
(38) Zhang, G.; Wu, C. *Macromol. Rapid Commun.* **2009**, *30*, 328−335.
(39) Höök, F.; Kasemo, B.; Nylander, T.; Fant, C.; Sott, K.; Elwing, H. *Anal. Chem.* **2001**, *73*, 5796−5804.

(40) Du, B.; Johannsmann, D. *Langmuir* **2004**, *20*, 2809−2812.
(41) Cao, Z.; Du, B.; Chen, T.; Li, H.; Xu, J.; Fan, Z. *Langmuir* **2008**, *24*, 5543−5551.
(42) Shen, L.; Chaudouet, P.; Ji, J.; Picart, C. *Biomacromolecules* **2011**, *12*, 1322−1331.
(43) Kobayashi, K.; Kamiya, S.; Enomoto, N. *Macromolecules* **1996**, *29*, 8670−8676.
(44) Loos, K.; Stadler, R. *Macromolecules* **1997**, *30*, 7641−7643.
(45) Mendoza, S. M.; Arfaoui, I.; Zanarini, S.; Paolucci, F.; Rudolf, P. *Langmuir* **2006**, *23*, 582−588.
(46) Ivashenko, O.; van Herpt, J. T.; Feringa, B. L.; Rudolf, P.; Browne, W. R. *Langmuir* **2013**, *29*, 4290−4297.
(47) Sauerbrey, G. *Z. Phys.* **1959**, *155*, 206−222.
(48) Ulman, A. *Chem. Rev.* **1996**, *96*, 1533−1554.
(49) Cuenot, S.; Gabriel, S.; Jerome, R.; Jerome, C.; Fustin, C.-A.; Jonas, A. M.; Duwez, A.-S. *Macromolecules* **2006**, *39*, 8428−8433.
(50) Flory, P. J. *Statistical Mechanics of Chain Molecules*; Hanser: Munich/Vienna/New York, 1989.
(51) Willet, N.; Duwez, A.-S. *Molecular Manipulation with Atomic Force Microscopy*; Taylor & Francis Group/CRC Press: Boca Raton, FL, 2011.
(52) Luzinov, I.; Julthongpiput, D.; Malz, H.; Pionteck, J.; Tsukruk, V. V. *Macromolecules* **2000**, *33*, 1043−1048.
(53) Fritz, M. C.; Hahner, G.; Spencer, N. D.; Burli, R.; Vasella, A. *Langmuir* **1996**, *12*, 6074−6082.
(54) Cheetham, N. W. H.; Tao, L. *Carbohydr. Polym.* **1998**, *35*, 287−295.
(55) Winter, W. T.; Sarko, A. *Biopolymers* **1974**, *13*, 1447−1460.
(56) Milani, A.; Aiman Fadel, N.; Brambilla, L.; Del Zoppo, M.; Castiglioni, C.; Zerbi, G.; Stradi, R. *J. Raman Spectrosc.* **2009**, *40*, 1110−1116.
(57) Tusch, M.; Kruger, J.; Fels, G. *J. Chem. Theory Comput.* **2011**, *7*, 2919−2928.
(58) Godet, M. C.; Bizot, H.; Buléon, A. *Carbohydr. Polym.* **1995**, *27*, 47−52.